IEEE Access
Multidisciplinary Rapid Review Open Access Journal

Received May 30, 2018, accepted June 30, 2018, date of publication July 4, 2018, date of current version July 25, 2018.

Digital Object Identifier 10.1109/ACCESS.2018.2853090

Adaptive PID Control of Wind Turbines for Power Regulation With Unknown Control Direction and Actuator Faults

HAMED HABIBI[1], HAMED RAHIMI NOHOOJI[1,2], AND IAN HOWARD[1]
[1]Faculty of Science and Engineering, School of Civil and Mechanical Engineering, Curtin University, Perth, WA 6845, Australia
[2]Center for Research in Mechatronics, Institute of Mechanics, Materials and Civil Engineering, Université catholique de Louvain, 1348 Louvain-la-Neuve, Belgium

Corresponding author: Hamed Habibi (hamed.habibi@postgrad.curtin.edu.au)

ABSTRACT Proportional integral derivative (PID) regulators are the most practical control schemes for industrial wind turbines. The key to PID design is the determination of the control parameter gains, which motivated our attempts to construct an adaptive PID control for wind turbines allowing auto-tuning of the gains without the need for trial and error processes. By equipping a novel PID-based fault-tolerant controller with a Nussbaum-type function, a robust adaptive and fault-tolerant control scheme is developed for wind turbines. Compared with available methods, the proposed controller has advantages, such as the ability for dealing with complete nonlinear dynamics of wind turbines, including model uncertainty, ability to ensure system stability by using an adaptive self-tuning gain algorithm, and robustness against wind speed variation. Furthermore, it has the ability to accommodate unexpected actuator faults and the accommodation of an unknown control direction. However, the salient feature of the proposed controller lies in its simple structure and inexpensive online computational demands while dealing with the nonlinear dynamics of wind turbines and unknown disturbances. It is shown that the proposed pitch angle controller remains continuous and smooth and all the closed-loop system signals are guaranteed to be uniformly ultimately bounded. Theoretical analysis and numerical simulations are presented to confirm the effectiveness of the proposed control strategy.

INDEX TERMS Adaptive PID controller, fault-tolerant, pitch control, self-tuning gains, unknown control direction, wind turbine power regulation.

NOMENCLATURE

B_{dt}	Drivetrain torsion damping
B_g	Generator bearing viscous friction
B_r	Rotor bearing viscous friction
B_t	Tower damping ratio
C_p	Power coefficient
C_q	Torque coefficient
C_t	Thrust coefficient
$C1, C2, C3,$ $C4, C5, C6$	Performance Criteria
$C_{\dot{\rho}}, C_{\dot{\Phi}}$	Positive unknown constants
D	Pitch actuator uncertainty
F	Pitch actuator dynamic
F_t	Aerodynamic thrust
G	Pitch actuator control direction
J_g	Generator shaft inertia
J_r	Rotor shaft inertia
K_{dt}	Drivetrain torsion stiffness
K_{OP}, K_{OI}, K_{OD}	Optimized controller gains
K_P, K_I, K_D	Industrial controller gains
K_t	Tower elasticity
M_t	Nacelle mass
N	Nussbaum type function
N_g	Drivetrain ratio
P_a	Aerodynamic power
P_g	Produced electrical power
$P_{g,rated}$	Rated power
R	Blade length
T_a	Aerodynamic torque
T_g	Generator torque
$T_{g,max}$	Maximum generator torque

$\dot{T}_{g,max}$	Maximum generator torque variation rate
$T_{g,min}$	Minimum generator torque
$\dot{T}_{g,min}$	Minimum generator torque variation rate
$T_{g,rated}$	Rated generator torque
$T_{g,ref}$	Reference generator torque
$T_{g,s}$	Measured generator torque
V	Lyapunov function
V_r	Effective wind speed
V_w	Free wind speed
Z	Tracking error filter
a_f	Unknown nonnegative constant
$\tilde{a}$	Estimation error
$\hat{a}$	Estimation of variable a
e_g	Generator tracking error
e_p	Power tracking error
e_r	Rotor tracking error
$\boldsymbol{x}$	State vector
x_t	Tower displacement
$\Delta\tilde{f}_{PAD}$	Pitch actuator dynamic change
Ξ	Unknown variable in (0, 1)
Φ	pitch actuator bias
$\bar{\Phi}$	Positive unknown constant
$\alpha_{f_1}, \alpha_{f_2}$	Fault indices
β	Blade pitch angle
β_{max}	Maximum pitch angle
$\dot{\beta}_{max}$	Maximum pitch angle variation rate
β_{min}	Minimum pitch angle
$\dot{\beta}_{min}$	Minimum pitch angle variation rate
β_{ref}	Reference pitch angle
β_s	Measured pitch angle
$\ddot{\beta}_s$	Measured pitch acceleration
β_u	Pitch angle control
β^*	Desired pitch angle
η_{dt}	Drivetrain efficiency
η_g	Generator efficiency
θ_g	Generator rotation angle
θ_r	Rotor rotation angle
θ_Δ	Drivetrain twist angle
λ	Positive design parameter
λ_D	Adaptive controller gain
λ_{D_0}	Constant controller gain
λ_{tsr}	Tip speed ratio
$\nu_{\omega_g}, \nu_{\omega_r}, \nu_{\dot{\omega}_r}, \nu_{T_{g,s}}, \nu_\beta, \nu_{\ddot{\beta}}$	Measurement noise
ξ_d	Pitch actuator damping ratio
ρ	Pitch actuator effectiveness
ρ_a	Air density
σ_0, σ_1	Positive design parameters
τ_g	Converter time delay
φ	Core-function
φ_f	Nonnegative function
ω_g	Generator speed
$\omega_{g,rated}$	Rated generator speed
$\omega_{g,s}$	Measured generator speed
ω_n	Pitch actuator natural frequency
ω_r	Rotor speed
$\omega_{r,rated}$	Rated rotor speed
$\omega_{r,s}$	Measured rotor speed
$\dot{\omega}_{r,s}$	Measured rotor acceleration

I. INTRODUCTION

Wind energy is considered one of the most promising types of renewable energy capable of supplying a major part of the ever-increasing world's power demand, and an appropriate alternative to fossil fuels with near zero environmental pollution [1]. Accordingly, the wind turbine generated power capacity is the key factor which should be kept at the desirable level to satisfactorily respond to the power demand and also, to manage the operational and maintenance costs. In the last decades, it has been demonstrated that the control system plays a vital role for managing the operation of the wind turbine at its desired load and speed curves with safe operation [1], [2]. In the low wind speed region, i.e. so-called partial load, the desired operation is to capture as much power as possible via generator torque control, [3], while in the high wind speed region, i.e. so-called full load, the wind turbine control aims to produce the rated power via blade pitch angle control [4] to avoid probable catastrophic operation and keep the wind turbine structure safe [5]. Thus, full load is considered as the power regulation region.

In the full load operation, the rotor speed should be kept at the rated one, to avoid over speeding and hazardous operation. The power regulation is fulfilled via regulating the blade pitch angle to change the aerodynamic torque applied to the rotor, and consequently, control rotor speed. On the other hand, long term operation in harsh environments with wind gusts, may lead to pitch actuator faults, which includes actuator abnormal behavior and effectiveness loss [6]. This issue has led to more frequent maintenance procedures being conducted, to remove fault effects and improve the overall wind turbine performance. Otherwise, either less power than the rated one is generated, or the rotor speed is increased excessively. However, increased maintenance work is too costly, especially for modern offshore wind turbines, due to their reachability difficulties and longer downtime [4]. So, it would be beneficial to add fault-tolerance capability to the controller to handle actuator faults, meanwhile keeping the overall performance at the desired level [7]. Indeed, fault-tolerant control design will make the system operate satisfactorily despite the presence of actuator faults and will lessen the need for further maintenance procedures [8].

Many research works have been conducted to control the wind turbines in their full load region, e.g., adaptive control [9], [10], optimal control [11], [12], evolutionary algorithms [13], [14], robust control [15] and fuzzy logic control [16], [17]. The detailed review of power regulation control techniques can be found in [2] and [18]. Even though numerous advanced control approaches have been presented for control of wind turbines, PID control is still considered as the preferred approach in engineering practice with some improvements, e.g. [4], [7], [19].

The main reason is the intuitiveness in concept and simplicity in design of the PID control structure. Regarding pitch actuator fault accommodation, different approaches have been used, such as, adaptive sliding mode fault-tolerant control [4], [20], robust linear parameter varying control [6], [7] and fuzzy Takagi-Sugeno control [21], [22], Kalman filter [23] and proportional multi-integral (PMI) observer [24]. In most of the related works [23], [25]–[29], the fault-tolerant control consists of two main steps, including fault detection and fault accommodation. In the fault detection step, the fault moment, location, type and size are needed to be accurately estimated. This information is then used in fault accommodation schemes to remove fault effects, mostly via reconfiguring the controller or signal correction [6]. Accordingly, the inaccurate fault information may lead to significant performance degradation and even instability. This issue is considerable in nonlinear systems with different sources of disturbances, uncertainties and noises, such as wind turbines [24]. On the other hand, one new approach has been proposed recently, i.e. the fault is adaptively estimated as a part of the designed controller [4], [20], [30], [31]. In this approach, because the fault estimation and accommodation are simultaneously conducted, the controller performance is sensitive to the design parameters [4]. It should be noted that in [7] and [32], the passive fault-tolerant control approach is utilized, in which the controller is designed to be robust against the considered set of faults, even in the fault free case. Consequently, the performance conservatism is inevitable in this approach [7]. It is worth noting that most of the approaches lack the implementation simplicity, which is one of the key factors for the wind turbine industry.

Nevertheless, though PID control gained wide attention in wind turbine control systems, there are at least two major limitations for PID control of such systems. First, in order to determine PID gains, an *ad-hoc* and painstaking process is required. Hence, in spite of the various existing methods for tuning PID gains [17], [19], [33]–[35], there exists no systematic way in the literature of wind turbine control to determine such gains which ensure system stability and performance. Second, the available PID controls are generally effective only on linearized wind turbine models, but not for the entire nonlinear wind turbine behavior. This has led to controller designs based on the linearized model, assuming that the wind turbine is performing at its desired operational points, which is not necessarily the case in practice. Therefore, the resultant control which has been designed for the linearized wind turbine model, may not render the expected performance on the nonlinear model [36].

The *primary objective* of this paper is to solve the long-lasting problem of designing a PID controller for nonlinear wind turbines including determination of the gains analytically, and automatically while ensuring the stability. Since the proposed control scheme bears the general PID form, it has a simple structure and only requires low computational cost. However, differing from previous methods like linear parameter varying control [7], [34], or gain scheduling [33] which require linearization around different operational points, the presented control method is able to deal with the whole nonlinear dynamic behavior of wind turbines. In addition, to function satisfactorily and to provide acceptable performance for industrial applications, PID control gains will be properly designed and determined using the stability guaranteed Lyapunov-based algorithm. Thus, the presented approach does not involve a trial and error process or require manual tuning. Also, compared to previous works like fuzzy-logic which depend largely on designer skills, e.g., in defining fuzzy rules [17], [19], [22], we present systematic means for self-tuning the PID gains analytically. The proposed control method is also able to tolerate both additive, i.e., bias, and multiplicative, i.e., effectiveness loss on the pitch actuator and is robust to modeling uncertainties. The *secondary objective* of this paper is to find the method of effectively handling the unknown control direction followed by unpredictable wind speed variation without requiring wind speed measurement. In reality, the aerodynamic torque of wind turbines is a nonlinear function of pitch angle and wind speed. Thus, as wind speed variation is unpredictable, the control direction is not known as a priori which poses a significant challenge in the control of wind turbines [37]. Although several approaches have been reported on wind speed estimation [30], [38] or aerodynamic torque estimation [9], [31], resultant solutions are very complicated, which is not favorable in practice. Also, designing the pitch controller to be robust against wind speed variation, as in [15] and [39], may lead to some degree of conservatism. To the best of the authors' knowledge, although a vast amount of research results on the control of wind turbines with unknown wind speed have been suggested in the literature, there is still a need for a systematic method to cope with the unknown control direction of the wind turbines without requiring wind speed measurement or estimation. Accordingly, in this paper, we introduce the use of the Nussbaum-type function for the control design of the wind turbines to cope with the unpredictable wind speed variation and the resultant unknown control direction.

The rest of the paper is organized as follows. In Section II, the nonlinear wind turbine model, including pitch actuator faults, is introduced. Considering the desired operation of the wind turbine in the full load region, the combined rotor dynamic model is derived, in Section III. Accordingly, in Section IV, the proposed controller is designed. The numerical simulation results, using the proposed, industrial, and optimized gain PID controllers are given in Section V, where the comparison is made, and the effectiveness of the proposed controller is evaluated. Finally, the discussion, and conclusions are given in Sections VI and VII, respectively.

II. WIND TURBINE MODEL

The wind turbine blades capture kinetic energy available in the wind and transfers it into the rotor shaft, rotating with speed ω_r. Interactions between the effective wind speed, V_r, and the blades causes an aerodynamic torque, T_a, and thrust,

F_t, on the rotor. Aerodynamic torque and thrust are stated as [20],

$$T_a = \frac{1}{2}\rho_a \pi R^3 V_r^2 C_q(\beta, \lambda_{tsr})$$
$$F_t = \frac{1}{2}\rho_a \pi R^2 V_r^2 C_t(\beta, \lambda_{tsr}), \quad (1)$$

respectively, where, ρ_a and R are air density and blade length, respectively. C_q is the torque coefficient and C_t is the thrust coefficient, both functions of blade pitch angle, β, and tip speed ratio, λ_{tsr}. Also, λ_{tsr} is defined as $\lambda_{tsr} = R\omega_r/V_r$ [1]. Aerodynamic thrust causes a fore-aft oscillation of the nacelle, considering an elastic tower. Tower dynamics are given in Appendix A. Considering the velocity of the nacelle, i.e. $\dot{x}_t$, and free wind speed, V_w, i.e. the wind speed before encountering the blades, the effective wind speed at the rotor plane is stated as $V_r = V_w - \dot{x}_t$ [9]. The power harvested by the blades and transferred into the rotor shaft, is stated as

$$P_a = \frac{1}{2}\rho_a \pi R^2 V_r^3 C_p(\beta, \lambda_{tsr}), \quad (2)$$

where, C_p is the power coefficient. Also, considering $P_a = T_a\omega_r$, the relation between power and torque coefficients, is, $C_p = C_q\lambda_{tsr}$.

The empirical equations of C_p and C_t are given in Appendix B. The rotor speed ω_r is increased via the drivetrain and transferred into the generator shaft, rotating at ω_g. Drivetrain and generator models are described in Appendix A. The electrical power P_g is produced in the generator which is given by,

$$P_g = \eta_g \omega_g T_g, \quad (3)$$

where, η_g is the generator efficiency and T_g is the generator shaft torque. In full load operation it is aimed to keep P_g at the rated value $P_{g,rated}$. In fact, the available wind energy, in this region, is higher than the wind turbine rated power, but to keep the wind turbine safe structurally, $P_{g,rated}$ is only requested [4], [5]. In this regard, considering (3), *(i)* T_g is to be fixed at the rated value $T_{g,rated}$, and *(ii)* ω_g is to be maintained at its rated value $\omega_{g,rated}$ to achieve the rated power generation as, $P_g = \eta_g T_g \omega_g = \eta_g T_{g,rated}\omega_{g,rated} = P_{g,rated}$ [7], [27]. The objective *(i)* is simply achieved by setting the generator reference torque, i.e. $T_{g,ref}$, at $T_{g,rated}$ and due to the fast response of the generator dynamics, this leads T_g to follow $T_{g,ref}$, rapidly. The objective *(ii)* is attained by regulating the blade pitch angle via the pitch actuator to vary the applied aerodynamic torque, and consequently, rotor speed. Accordingly, this leads to regulating the generator speed, considering the drivetrain model. See Appendix A for more information. As the power regulation of the wind turbine is considered in this paper, the generator torque controller is not active [4]. Accordingly, the faults in the generator are not considered and it is assumed that these faults have already been accommodated using the generator torque controller, which is not within the scope of this paper.

The pitch actuator is a hydraulic mechanism to rotate the blades and adjust the pitch angle to the reference pitch angle, β_{ref}, commanded by the pitch controller. The pitch actuator is modelled as a second order dynamic system as [4],

$$\ddot{\beta} = -\omega_n^2\beta - 2\omega_n\xi_d\dot{\beta} + \omega_n^2\beta_{ref}, \quad (4)$$

where, ω_n is natural frequency and ξ_d is damping ratio of the pitch actuator. Considering the available industrial wind turbines, the limited operational ranges of the pitch actuator are as $\dot{\beta}_{min} \leq \dot{\beta} \leq \dot{\beta}_{max}, \beta_{min} \leq \beta \leq \beta_{max}$. It should be noted that $(\bullet)_{max}$ and $(\bullet)_{min}$ stand for maximum and minimum allowable value of the variable $(\bullet)$, respectively. The measured pitch angle and its derivative are modelled as $\beta_s = \beta + \nu_\beta$, $\ddot{\beta}_s = \ddot{\beta} + \nu_{\ddot{\beta}}$, where ν_β and $\nu_{\ddot{\beta}}$ are the noise contents [5]. Long term operation of the pitch actuator, with reduced maintenance action, may lead to changes in the dynamic behaviour of the pitch actuator, effectiveness loss and bias. The three most reported pitch actuator dynamic changes include high air content in the oil, pump wear and hydraulic leakage [7]. These dynamic changes lead to slower response speeds of the pitch actuator and, consequently, poor power regulation under full load operation. The dynamic change effects on the pitch actuator can be seen as a change of natural frequency and damping ratio in (4). The characteristics of these changes are summarized in Table 1 [4], [7], in which N, HAC, PW and HL represent normal, high air content, pump wear, hydraulic leakage situations, respectively. Also, $\omega_{n,X}$ is natural frequency and ξ_X is damping ratio in the situation X. α_{f_1} and α_{f_2} are fault indices.

TABLE 1. Pitch actuator dynamic change characteristics [4], [7].

	Natural Frequency (rad/s) and Damping Ratio	Fault Indicator
Normal	$\omega_{n,N} = 11.11$, $\xi_N = 0.6$	$\alpha_{f_1} = \alpha_{f_2} = 0$
Pump Wear	$\omega_{n,PW} = 7.27$, $\xi_{PW} = 0.75$	$\alpha_{f_1} = 0.63$, $\alpha_{f_2} = 0.30$
Hydraulic Leak	$\omega_{n,HL} = 3.42$, $\xi_{HL} = 0.9$	$\alpha_{f_1} = 1$, $\alpha_{f_2} = 0.88$
High Air Content	$\omega_{n,HAC} = 5.73$, $\xi_{HAC} = 0.45$	$\alpha_{f_1} = 0.81$, $\alpha_{f_2} = 1$

The effect of these dynamic changes is illustrated in Fig. 1, in which the initial pitch angle is set to 5° and $\beta_{ref} = 0°$,

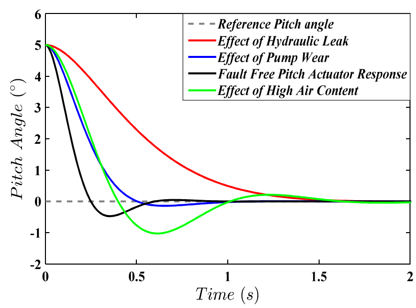

FIGURE 1. Dynamic change effects on pitch actuator response.

considering (4). It is obvious that the settling time for all dynamic change situations are slower than the normal one.

The dynamic change in the pitch actuator can be considered as an uncertainty which should be handled by the designed pitch angle controller and can be augmented into the pitch dynamic model as a convex function of normal values of natural frequency and damping ratio [40]. So, the pitch actuator model (4) can be rewritten including the dynamic change effect, i.e. added as uncertainty, to give,

$$\ddot{\beta} = -\omega_{n,N}^2\beta - 2\omega_{n,N}\xi_N\dot{\beta} + {\omega_{n,N}}^2\beta_{ref} + \Delta\tilde{f}_{PAD}, \quad (5)$$

where, $\Delta\tilde{f}_{PAD} = -\alpha_{f_1}\Delta(\tilde{\omega}_n^2)\beta - 2\alpha_{f_2}\Delta\left(\tilde{\omega}_n\tilde{\xi}\right)\dot{\beta} + \alpha_{f_1}\Delta(\tilde{\omega}_n^2)\beta_{ref}$, $\Delta(\tilde{\omega}_n^2) = \omega_{n,HL}^2 - \omega_{n,N}^2$ and $\Delta\left(\tilde{\omega}_n\tilde{\xi}\right) = \omega_{n,HAC}\xi_{HAC} - \omega_{n,N}\xi_N$.

During operation in harsh environments, the pitch actuator can be corrupted due to unanticipated faults, considered as bias and/or effectiveness loss which deviates the pitch angle from the expected one [6]. The effectiveness loss and bias of the pitch actuator can be modelled as,

$$\beta_u(t) = \rho(t)\,\beta_{ref}(t) + \Phi(t), \quad (6)$$

where, β_u is the actual pitch angle applied to the pitch actuator, $\Phi(t)$ represents the unknown uncontrollable pitch actuator bias that causes an unbalanced rotor rotation, and consequently, higher probability of the drivetrain fatigue [22]. Also, $\rho(t)$ is an unknown effectiveness of the actuator which is $0 < \rho(t) \leq 1$, where $\rho(t) = 1$ indicates healthy pitch actuator and $\rho(t) = 0$ refers to total actuator loss [16], [22]. The pitch actuator dynamic response, (5), combined with dynamic change uncertainty, pitch actuator bias and effectiveness loss, can be rewritten as,

$$\begin{aligned}\ddot{\beta} &= -\omega_{n,N}^2\beta - 2\omega_{n,N}\xi_N\dot{\beta} \\ &\quad + \omega_{n,N}^2\left(\rho(t)\,\beta_{ref} + \Phi(t)\right) + \Delta\tilde{f}_{PAD}, \quad (7)\end{aligned}$$

which will be considered in the design of the proposed controller in Section IV.

III. WIND TURBINE DESIRABLE OPERATIONAL DYNAMIC BEHAVIOR

Considering the wind turbine operation, it is desirable to keep the drivetrain torsion angle variation $\dot{\theta}_\Delta$ as small as possible, which, consequently, leads to reduction in the drivetrain stress. $\dot{\theta}_\Delta$ is defined as $\dot{\theta}_\Delta = \omega_r - \omega_g/N_g$, where N_g is the drivetrain ratio. Accordingly, $\dot{\theta}_\Delta = 0$ leads to $N_g\omega_r = \omega_g$. So, it is desirable to keep the rotor and generator speeds proportional to the drivetrain ratio [18], [41]. On the other hand, as generator speed is aimed to be maintained at $\omega_{g,rated}$, rotor speed is to be maintained at $\omega_{g,rated}/N_g$ [36]. Considering $\dot{\theta}_\Delta = 0$ with zero initial drivetrain torsion angle, leads to $\theta_\Delta = 0$ as the reduced drivetrain stress trajectory [36]. The desirable operational dynamic equation of the wind turbine with reduced drivetrain stress can be stated as [18], [36],

$$\begin{aligned}\dot{\omega}_r &= a_1\omega_r + a_2\omega_g + a_3T_a \\ \dot{\omega}_g &= b_1\omega_r + b_2\omega_g + b_3T_g, \quad (8)\end{aligned}$$

where, $a_1 = -(B_{dt} + B_r)/J_r$, $a_2 = B_{dt}/N_gJ_r$, $a_3 = 1/J_r$, $b_1 = \eta_{dt}B_{dt}/N_gJ_g$, $b_2 = \left(-\eta_{dt}B_{dt}/N_g^2 - B_g\right)/J_g$, $b_3 = -1/J_g$. Also, J_r and J_g are the inertia of rotor and generator shafts, which are rotating at speeds ω_r and ω_g, respectively. B_{dt} is the torsion damping of the drivetrain. Also, viscous frictions for rotor and generator shaft bearings are considered whose coefficients are B_r and B_g, respectively. η_{dt} is the drivetrain efficiency in transferring speed. Accordingly, the second-time derivation of rotor speed can be given as,

$$\ddot{\omega}_r = c_1\omega_r + c_2\omega_g + c_3T_a + c_4T_g + a_3\dot{T}_a, \quad (9)$$

where, $c_1 = a_1^2 + a_2b_1$, $c_2 = a_1a_2 + a_2b_2$, $c_3 = a_1a_3$, $c_4 = a_2b_3$, forms the combined rotor dynamic behavior model. Considering (9), it is obvious that the rotor speed and generator speed, are controlled by the pitch angle regulation. It is assumed that in the vicinity of any triple pair (V_r, ω_r, β) in the operational range of the wind turbine, T_a is not a singular function. Also, there is a given β^* for any pair of (V_r, ω_r), such that it steers the wind turbine to the rated power generation, by adjusting the pitch angle as $\beta = \beta^*$ [9]. Accordingly, as the wind speed varies, β^* will take the corresponding value to satisfy the desirable performance. A diagram of β^* for the considered wind turbine benchmark model in the full load region, as obtained in [7], is illustrated in Fig. 2. It should be noted that, as the wind speed is considered as an unmeasurable and uncontrollable disturbance, β^* is the unknown variable. Thus, the pitch angle cannot be simply set at β^*, but instead, it is regulated by the designed pitch controller.

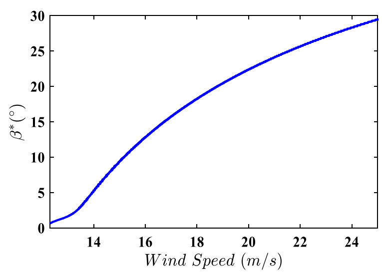

FIGURE 2. Diagram of β^* in full load operation.

Assumption 1: In this paper, it is assumed that the blade aerodynamic characteristics are not varied due to the environmental effect such as debris, ice and dust on the blades. So, $T_a(V_r, \omega_r, \beta^*)$ and β^* for any given pair (V_r, ω_r), are constant through time [7], [36]. Also, in the case of any potential change, it would be very slow which lies within the yearly scheduled maintenance procedure of the wind turbine and then its effects will be removed soon enough before the occurrence of any significant change [7].

Considering (1), T_a is a non-affine function of pitch angle [9]. One obvious solution is linearization, which leads to model inaccuracies. To avoid such inaccuracies, in this paper the mean value theorem is utilized.

According to this approach, for any given pair of (V_r, ω_r), there exists $\Xi \in (0, 1)$ such that [9],

$$T_a(V_r, \omega_r, \beta) = T_a(V_r, \omega_r, \beta^*) + (\beta - \beta^*) \left.\frac{\partial T_a}{\partial \beta}\right|_{(V_r, \omega_r, \beta_k)}, \tag{10}$$

where, $\beta_k = \Xi\beta + (1 - \Xi)\beta^*$. The $\partial T_a/\partial\beta$ diagram in the full load region, considering the C_p surface in Appendix B, is shown in Fig. 3.

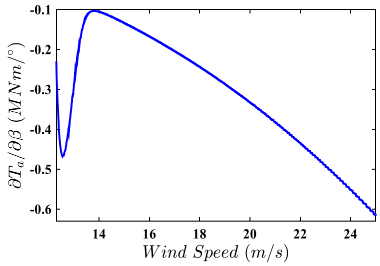

FIGURE 3. $\partial T_a/\partial\beta$ **diagram in full load operation.**

Remark 1: In Fig. 3, it is obvious that $-L \leq \partial T_a/\partial\beta \leq -U < 0$, where, $0 < U < L$, which implies that, as the wind speed increases, with increasing pitch angle, the applied aerodynamic torque will decrease, to prevent the rotor from over speeding.

Considering Assumption 1, time derivative of (10) leads to,

$$\dot{T}_a(V_w, \omega_r, \beta) = \dot{\beta}\frac{\partial T_a}{\partial \beta} = \dot{\beta}\, T_a)_\beta, \tag{11}$$

where, $T_a)_\beta$ is used to represent $\frac{\partial T_a}{\partial \beta}$. Now, replacing (11) into (9), one can obtain,

$$\ddot{\omega}_r = c_1\omega_r + c_2\omega_g + c_3T_a + c_4T_g + a_3\dot{\beta}\, T_a)_\beta, \tag{12}$$

In this paper, the wind turbine dynamic states of interest are the vector $\boldsymbol{x}\ \mathcal{D}\ [\omega_r, \omega_g, \beta, T_g]^T$. Substituting (7) in (12) leads to,

$$\ddot{\omega}_r = F(\boldsymbol{x},t) + G(\boldsymbol{x},t)\left(\rho(t)\,\beta_{ref} + \Phi(t)\right) + D(\boldsymbol{x},t), \tag{13}$$

where, $F(\bullet) = c_1\omega_r + c_2\omega_g + c_3T_a + c_4T_g - \omega_{n,N}a_3\, T_a)_\beta\, \beta/2\xi_N - a_3\, T_a)_\beta\, \ddot{\beta}/2\omega_{n,N}\xi_N$, $G(\bullet) = \omega_{n,N}a_3\, T_a)_\beta/2\xi_N$ and $D(\bullet)\, a_3\, T_a)_\beta\, \Delta\tilde{f}_{PAD}/2\omega_{n,N}\xi_N$.

Considering (13), it is obvious that the combined rotor dynamic model is in an affine form of input pitch angle β_{ref}. $F(\bullet)$ is not completely known, because of the existence of the $T_a)_\beta$ term and noise contents of variable measurements which appear in $F(\bullet)$. Also, it is important to be mentioned that the control direction of $G(\bullet)$ is an unknown function, due to the existence of $T_a)_\beta$ which depends on wind speed. To handle this issue we utilize the Nussbaum function, which is a well-known tool to cope with an unknown control direction issue. Finally, $D(\bullet)$ is the unknown pitch actuator model uncertainty.

Remark 2: Considering Fig. 3 and Remark 1, it is obvious that $G(\bullet) = \omega_{n,N}a_3T_a)_\beta/2\xi_N$ takes value in $-\omega_{n,N}a_3L/2\xi_N \leq G(\bullet) \leq -\omega_{n,N}a_3U/2\xi_N$ and also $G(\bullet) \neq 0$ for any triple pair (V_r, ω_r, β).

Assumption 2: Considering the bounded achievable pitch angle β and it is allowable variation rate $\dot{\beta}$, it is assumed $|\Phi| \leq \bar{\Phi} < \infty$, $|\dot{\rho}| \leq C_{\dot{\rho}} < \infty$ and $|\dot{\Phi}| \leq C_{\dot{\Phi}} < \infty$, where $\bar{\Phi}$, $C_{\dot{\rho}}$ and $C_{\dot{\Phi}}$ are positive unknown constants [6].

Assumption 3: Considering information extraction from system nonlinearities [42], there is an unknown nonnegative constant a_f and computable nonnegative function $\varphi_f(\boldsymbol{x})$ such that it satisfies $|F(\boldsymbol{x},t) + \Phi(t)\,G(\boldsymbol{x},t) + D(\boldsymbol{x},t)| \leq a_f\varphi_f(\boldsymbol{x})$ [6].

Assumption 4: In this paper the measurement noise on the variable of Y, i.e. ν_Y, is considered bounded by an unknown bound $\bar{d}_Y$, which is a practical assumption [29].

IV. PID-LIKE PROPOSED CONTROLLER CONSTRUCTION

The proposed controller is designed to regulate pitch angle and maintain the rotor speed at the rated one, in the presence of wind speed variation and to attenuate model uncertainty, disturbance, and pitch actuator faults. It is aimed to utilize the PID control structure with automatic adaptive gain tuning. A Nussbaum-type function is augmented in the adaptive laws to take the unknown control direction into consideration. Finally, stability of the wind turbine model augmented with the proposed controller in the presence of wind speed variation is proved analytically. Now, to construct the proposed controller, the rotor tracking error and its first-time derivative are defined as,

$$\begin{aligned} e_r(t) &= \omega_{r,s}(t) - \omega_{r,rated} \\ \dot{e}_r(t) &= \dot{\omega}_{r,s}(t) - \dot{\omega}_{r,rated}. \end{aligned} \tag{14}$$

$\omega_{r,s}$ is rotor speed measurement as, $\omega_{r,s} = \omega_r + \nu_{\omega_r}$ and $\dot{\omega}_{r,s}$ is rotor acceleration measurement as, $\dot{\omega}_{r,s} = \dot{\omega}_r + \nu_{\dot{\omega}_r}$. ν_{ω_r} and $\nu_{\dot{\omega}_r}$ are noise contents of each sensor. Since the rated rotor speed of the wind turbine is assumed to be a constant value, then $\dot{\omega}_{r,rated} = 0$ [4]. Taking the second time derivative of e_r, takes the combined rotor dynamic model (13) into consideration, as,

$$\ddot{e}_r = F(\bullet)\, G(\bullet)\left(\rho(t)\,\beta_{ref} + \Phi(t)\right) + D(\bullet). \tag{15}$$

To proceed, the tracking error filter is defined as,

$$Z(t) = 2\lambda e_r(t) + \lambda^2\int_0^t e_r(\tau)\,d\tau + \dot{e}_r(t), \tag{16}$$

where, λ is a positive design parameter such that the transfer function $s^2 + 2\lambda s + \lambda^2$ is Hurwitz. Note that the filtered error $Z(t)$, is formed by combination of proportional, integral and derivative terms of the tracking error $e_r(t)$ which is the basis of our PID control design. Considering (15) and (16), it can be easily shown that,

$$\dot{Z} = H(\boldsymbol{x},t) + B(\boldsymbol{x},t)\,\beta_{ref}, \tag{17}$$

where, $B(\boldsymbol{x},t) = \rho(t)\,G(\boldsymbol{x},t)$ and $H(\boldsymbol{x},t) = 2\lambda\dot{e}_r(t) + \lambda^2 e_r(t) + F(\boldsymbol{x},t) + \Phi(t)\,G(\boldsymbol{x},t) + D(\boldsymbol{x},t) + \lambda^2\nu_{\omega_r} + 2\lambda\nu_{\dot{\omega}_r}$.

Considering Assumptions 3 and 4, then, it can be shown that $H(\bullet)$ is upper bounded as,

$$|H(\bullet)| = 2\lambda |\dot{e}_r| + \lambda^2 |e_r| + a_f \varphi_f(\boldsymbol{x}) + \lambda^2 \bar{d}_{\omega_r} + 2\lambda \bar{d}_{\dot{\omega}_r} < a\varphi(\boldsymbol{x}), \quad (18)$$

where, $a = max\left\{a_f, 2\lambda, \lambda^2, \lambda^2 \bar{d}_{\omega_r} + 2\lambda \bar{d}_{\dot{\omega}_r}\right\}$ is an unknown positive constant and $\varphi(\boldsymbol{x}) = \varphi_f(\boldsymbol{x}) + |\dot{e}_r| + |e_r| + 1$. It should be noted that $\varphi(\boldsymbol{x})$ is called a core-function and is a computable scalar function [42]. It can be proved that boundedness of Z leads to boundedness of e_r, $\int_0^t e_r(\tau)\,d\tau$ and $\dot{e}_r$. So, the controller is designed to ensure Z is uniformly ultimately bounded (UUB) [43]. In this regard, the following definition and lemma are stated, on which basis the controller is designed, and its stability is proved.

Definition 1: Any smooth continuous even function $N(\xi(t))$ is called a Nussbaum-type function, if $\sup \frac{1}{r}\int_0^r N(\xi)\,d\xi = +\infty$ and $\lim_{t\to\infty} \inf \frac{1}{r}\int_0^r N(\xi)d\xi = -\infty$ [6].

Lemma 1: Assume $V(t) > 0$ and $\xi(t)$ are smooth defined functions defined on the time interval $[0\, t_f)$. Also, $N(\xi(t))$ is a selected Nussbaum-type function. Then, for any $t \in [0\, t_f)$, if $V(t) < c_0 + e^{-c_1 t}\int_0^t (g(\tau)N(\xi(\tau)) + 1)\,\dot{\xi} e^{c_1\tau}d\tau$ holds true, where c_0 and c_1 are positive constants, and $g(\tau)$ represents a time-varying parameter, which takes values in the unknown closed intervals $L \in [1^+, 1^-]$ with $0 \notin L$, then $V(t)$, $\xi(t)$ and $\int_0^t g(\tau)N(\xi(\tau))\dot{\xi}e^{c_1\tau}d\tau$ must be bounded on $[0 t_f)$ [44].

A PID-like pitch angle controller is proposed as,

$$\beta_{ref} = \left(\lambda_{D_0} + \lambda_D\right) N(\xi) Z(t), \quad (19)$$

where, λ_{D_0} is a positive design parameter. Also, in (19), the controller gain λ_D is obtained via the following adaptive laws,

$$\begin{aligned} \lambda_D &= \hat{a}\varphi^2 \\ \dot{\xi} &= \left(\lambda_{D_0} + \lambda_D\right) Z^2 \\ \dot{\hat{a}} &= -\sigma_0 \hat{a} + \sigma_1 \varphi^2 Z^2, \end{aligned} \quad (20)$$

where, σ_0 and σ_1 are positive design parameters, and $\hat{a}$ is the estimation of a.

Remark 3: The proposed controller (19) can be seen as a combination of two parts, i.e. $Z(t)$ and $\left(\lambda_{D_0} + \lambda_D\right) N(\xi)$. Considering (16), it is obvious that $Z(t)$ is a PID-like filter of the tracking error and on the other hand, $\left(\lambda_{D_0} + \lambda_D\right) N(\xi)$ is auto-updating the gains of $Z(t)$. This is the reason the proposed controller is called a PID-like controller.

The stability of the wind turbine model using the proposed controller is proved via the following theorem.

Theorem 1: Consider the combined rotor dynamic model (13), including the presence of the pitch actuator fault and uncertainty. Under assumptions 1-4 and the unmeasured wind speed variation, using the proposed pitch angle controller (19) with adaptive laws (20); the rated rotor speed tracking error is guaranteed to be UUB, all the internal signals are UUB, and pitch angle controller signal is smooth everywhere.

Proof: Let the Lyapunov function V be selected as,

$$V = \frac{1}{2}Z^2 + \frac{1}{2\sigma_1}\tilde{a}^2, \quad (21)$$

where, $\tilde{a}$ is estimation error of a, defined as $\tilde{a} = a - \hat{a}$. The time derivative of (21), considering (17) and (19), is derived as,

$$\dot{V} = Z\dot{Z} - \frac{1}{\sigma_1}\tilde{a}\dot{\hat{a}} = ZH(\bullet) + B(\bullet)\left(\lambda_{D_0} + \lambda_D\right) N(\xi) Z^2 + \frac{\sigma_0}{\sigma_1}\hat{a}\tilde{a} - \tilde{a}\varphi^2 Z^2. \quad (22)$$

Considering the trivial inequality $(\tilde{a} - a)^2 \geq 0$, it can be easily shown that $\hat{a}\tilde{a} \leq a^2/2 - \tilde{a}^2/2$. Also, considering (18), $ZH < |Z|\,a\varphi < a\varphi^2 Z^2 + a/4$ holds true. So, $\dot{V}$ can be bounded as,

$$\dot{V} \leq a\varphi^2 Z^2 + \frac{a}{4} + B(\bullet)(\xi)\,\dot{\xi} + \frac{\sigma_0}{\sigma_1}\frac{a^2}{2} - \frac{\sigma_0}{\sigma_1}\frac{\tilde{a}^2}{2} - \tilde{a}\varphi^2 Z^2. \quad (23)$$

The right hand side of (23) is equal to $\left(\hat{a}\varphi^2 + \lambda_{D_0}\right) Z^2 + \frac{a}{4} + B(\cdot)\,N(\xi)\,\dot{\xi} + \frac{\sigma_0}{\sigma_1}\frac{a^2}{2} - \frac{\sigma_0}{\sigma_1}\frac{\tilde{a}^2}{2} - \lambda_{D_0} Z^2$. Also considering $\lambda_D = \hat{a}\varphi^2$ and $\dot{\xi} = \left(\lambda_{D_0} + \lambda_D\right) Z^2$, (23) yields,

$$\dot{V} \leq \dot{\xi} + B(\cdot)\,N(\xi)\,\dot{\xi} + \frac{a}{4} + \frac{\sigma_0}{\sigma_1}\frac{a^2}{2} - \frac{\sigma_0}{\sigma_1}\frac{\tilde{a}^2}{2} - \lambda_{D_0} Z^2 < \dot{\xi} + B(\cdot)\,N(\xi)\,\dot{\xi} - c_1 V + c_2, \quad (24)$$

where, $c_2 = \min(\sigma_0, 2\lambda_{D_0})$ and $c_2 = a/4 + \sigma_0 a^2/2\sigma_1$ and both are positive. MultiplyingNussbaum-type function, used in (24) by $e^{c_1 t} > 0$, yields

$$d\left(Ve^{c_1 t}\right)/dt \leq \dot{\xi}e^{c_1 t} + B(\cdot)\,N(\xi)\,\dot{\xi}e^{c_1 t} + c_2 e^{c_1 t}, \quad (25)$$

and integrating both sides of (25) over $[0\, t]$, leads to

$$V < e^{-c_1 t}\int_0^t (B(\cdot)\,N(\xi) + 1)\,\dot{\xi}e^{c_1\tau}d\tau + \left(V(0) - \frac{c_2}{c_1}\right)e^{-c_1 t} + \frac{c_2}{c_1}. \quad (26)$$

Since $0 < e^{-c_1 t} \leq 1$, the inequality (26) can be rewritten as,

$$V < e^{-c_1 t}\int_0^t (B(\cdot)\,N(\xi) + 1)\,\dot{\xi}e^{c_1\tau}d\tau + c_0, \quad (27)$$

where, $c_0 = c_2/c_1 + V(0)$ is a positive constant. Considering Lemma 1 and Remark 2, it is concluded from (27) that V, ξ and $\int_0^t (B(\cdot)\,N(\xi) + 1)\,\dot{\xi}e^{c_1\tau}d\tau$ are bounded on $[0\, t)$. Thus, the closed-loop system solution is UUB. Boundedness of V leads to boundedness of Z and $\tilde{a}$. Because a is bounded and $\tilde{a} = a - \hat{a}$, then $\hat{a}$ is bounded. Since, $V(0)$ is bounded, it is obvious that $\lim_{t\to+\infty} Z^2/2 \leq c_2/c_1$; i.e. $|Z|$ converges to the set $\Omega = \{|Z|\,|\,|Z| < \sqrt{2c_2/c_1}\}$ as $t \to +\infty$. On the other hand, boundedness of Z ensures boundedness of e_r, $\int_0^t e_r(\tau)\,d\tau$ and $\dot{e}_r$, and consequently, ω_r, ω_g, φ are bounded [43]. Therefore, from (17), (19) and (20), it can be stated that β_{ref}, $\dot{\hat{a}}$, $\dot{Z}$ and λ_D are bounded. Taking the time derivative of β_{ref}, (19), can be written as,

$$\dot{\beta}_{ref} = \frac{\partial\beta_{ref}}{\partial Z}\dot{Z} + \frac{\partial\beta_{ref}}{\partial N}\frac{\partial N}{\partial\xi}\dot{\xi} + \frac{\partial\beta_{ref}}{\partial\varphi}\dot{\varphi} + \frac{\partial\beta_{ref}}{\partial\hat{a}}\dot{\hat{a}}, \quad (28)$$

where, $\partial\beta_{ref}/\partial Z = (\lambda_{D_0}+\lambda_D)N(\xi)$, $\partial\beta_{ref}/\partial N = (\lambda_{D_0}+\lambda_D)Z(t)$, $\partial\beta_{ref}/\partial\varphi = 2\hat{a}\varphi N(\xi)Z(t)$, $\dot{\varphi} = (\partial\varphi/\partial\mathbf{x})\dot{x}+(\partial\varphi/\partial e)\dot{e}$ and $\partial\beta_{ref}/\partial\hat{a} = \varphi^2 N(\xi)Z(t)$. Note that Z, $\dot{Z}$, ξ, $\dot{\xi}$, $\hat{a}$, $\dot{\hat{a}}$, φ, $N(\xi)$ and, consequently, $\partial N/\partial\xi$ are all bounded and continuous. Accordingly, all terms in (28) are bounded and continuous. Thus, $\dot{\beta}_{ref}$ is bounded and continuous, which leads to smooth β_{ref}. This ends the proof. ■

V. EVALUATION OF THE PROPOSED CONTROLLER

In this section, the proposed pitch angle controller is evaluated via numerical simulations on a nonlinear wind turbine benchmark model [5], [10], [30]. Also, the results are compared to those from an industrial baseline controller (IBC) as well as an optimized-gain PID controller using moth-flame optimization (MFO-PID) which is elaborated in details in [45] to demonstrate the performance advantages of the proposed controller, in both fault free and faulty situations. Also, the performance criteria are introduced to quantify the performance of the wind turbine. It should be noted that all numeric values of the wind turbine benchmark model are given in Appendix C.

A. INDUSTRIAL BASELINE CONTROLLER

In this paper, a traditional PID controller is used to make the context of comparison to the proposed controller performance. Such a controller is designed to regulate the pitch angle based on the generator speed tracking error, which is defined as,

$$e_g(t) = \omega_{g,s}(t) - \omega_{g,rated}, \quad (29)$$

where, $\omega_{g,s} = \omega_g + \nu_{\omega_g}$, and ν_{ω_g} is the noise contents of each sensor. A traditional industrial baseline controller (IBC) is given by, [4], [7],

$$\beta_{ref}(t) = K_P e_g(t) + K_I\int_0^t e_g(\tau)\,d\tau + K_D\dot{e}_g(t), \quad (30)$$

where, K_P, K_I and K_D are proportional, integral and derivative controller gains, respectively which are set using traditional methods, to have system stability as well as satisfying performance. In this paper the IBC gains are as, $K_P = 1$, $K_I = 4$ and $K_D = 0$, which are obtained via trial and error processes, considering gain and phase stability margins [4], [28], [46]. One advantage of our proposed controller over the IBC (30), is to link the gains through the design parameter λ which makes the gain tuning process simpler compared to currently available controllers. Also, it has been proposed to filter the generator sensor, before feeding it into the PID controller to remove noise content and avoid amplification of noise via the controller gain. However, it is obvious that, in the structure of the controller (30), the sensor noise $\omega_{g,s}$ is not necessarily attenuated and may be amplified. Accordingly, in IBC K_D is set zero [4], [28]. Also, the pitch actuator uncertainty, i.e. $\Delta\tilde{f}_{PAD}$, is not analytically attenuated in this controller. On the other hand, any possible loss of effectiveness and bias, i.e. $\rho(t)$ and $\Phi(t)$ in (6), are not assured to be accommodated. So, it is beneficial to modify the current available industrial controller, firstly, to have industrial acceptability, and also, to satisfy the desired performance despite the presence of disturbances, uncertainties and faults. All the above modifications are considered in the development of the proposed controller (19).

B. MOTH-FLAME OPTIMIZED GAIN PID CONTROLLER

In [45], an optimized-gain PID pitch controller using the moth-flame optimization algorithm (MFO-PID) is considered and its results have been compared with the other optimization algorithms, including Zeigler Nichols, simplex algorithm and genetic algorithm. It has been demonstrated that the obtained gains using the moth-flame algorithm, led to the minimum performance objective. So, in this paper the performance of the proposed controller is compared to the performance of the MFO-PID. The pitch angle using the MFO-PID controller is structured as [45],

$$\beta_{ref}(t) = K_{OP}e_p(t) + K_{OI}\int_0^t e_p(\tau)\,d\tau + K_{OD}\dot{e}_p(t), \quad (31)$$

where, $e_p(t) = P_g(t) - P_{g,rated}$ is power tracking error. K_{OP}, K_{OI} and K_{OD} are proportional, integral and derivative optimized controller gains, obtained for the generic nonlinear wind turbine model, respectively, as, $K_{OP} = 0.179$, $K_{OI} = 0.458$ and $K_{OD} = 0.033$ [45]. It should be noted that the MFO-PID gains are obtained based on power tracking error, while the IBC gains are based on generator speed tracking error. Accordingly, the MFO-PID gains are smaller than the IBC gains [45].

C. PERFORMANCE CRITERA

In full load operation, numerical criteria are used to quantify the performance of the wind turbine [5], [45]. As stated earlier, the generator speed is to be kept at the rated value, accordingly, we choose the difference between these two as the first criterion, as,

$$C1 = \int_0^{t_f}\left(w_g(\tau) - w_{g,rated}\right)^2 d\tau, \quad (32)$$

where, t_f is the execution time. Similar criterion is used for differences between the generated and rated power, as,

$$C2 = \int_0^{t_f}\left(P_g(\tau) - P_{g,rated}\right)^2 d\tau. \quad (33)$$

It is obvious that the aim is to keep $C1$ and $C2$ as close to zero as possible. On the other hand, the maximum deviation of the generated power from rated power is calculated as,

$$C3 = max\left(\left|P_g(t) - P_{g,rated}\right|\right). \quad (34)$$

Indeed, $C3$ represents the instantaneous generated power deviation from the rated value which may lead to sudden catastrophic break down, in contrast to $C2$ which accumulates all power deviation, which may lead to gradual failure. Also, the drivetrain torsion angle is calculated as,

$$C4 = \int_0^{t_f} \dot{\theta}_\Delta(\tau)^2 d\tau. \tag{35}$$

Considering reduced drivetrain stress, as described in Section IV, it is desired to keep $C4$ as close as possible to zero. Finally, to consider limited operational ranges of the possible pitch angle, which may lead to pitch actuator saturation, $C5$ and $C6$ are defined as,

$$\begin{aligned} C5 &= max\left(|\beta(t)|\right) \\ C6 &= max\left(\left|\dot{\beta}(t)\right|\right), \end{aligned} \tag{36}$$

which should not violate the given ranges.

D. NUMERICAL RESULTS

In this section, to verify the proposed controller performance, numerical simulations are conducted, and the results are compared to the IBC (30), and the MFO-PID (31) responses. Firstly, the performance of all controllers in normal situations, i.e. without pitch actuator effectiveness loss, bias or dynamic change, are carried out. Then, for each mentioned situation, the wind turbine operation is studied and also, the performance criteria are analyzed.

Considering the adaptive laws (20), and the inequality (18), the function φ_f should be selected appropriately. In this regard, considering (13) and Assumption 3, φ_f is selected as,

$$\begin{aligned} \varphi_f = &\left|c_1\omega_r\right| + \left|c_2\omega_g\right| + c_3\left(\frac{N_g T_{g,max}}{\eta_{dt}}\right) + \left|c_4 T_g\right| \\ &+ \left|\frac{\omega_{n,N} a_3 U \beta}{2\xi_N}\right| + \left|\frac{a_3 U \ddot{\beta}}{2\omega_{n,N}\xi_N}\right| + \left|\frac{\omega_{n,N} a_3 U}{2\xi_N}\right| \\ &+ \left|\frac{a_3 U \Delta\left(\tilde{\omega}_n \tilde{\xi}\right)\dot{\beta}}{\omega_{n,N}\xi_N}\right| + \left|\frac{a_3 U \Delta(\tilde{\omega}_n^2)\left(\beta_{max} - \beta_{min}\right)}{2\omega_{n,N}\xi_N}\right|, \end{aligned} \tag{37}$$

which is obviously a computable scalar function, as a part of the controller structure and, $\varphi = \varphi_f + |\dot{e}_r| + |e_r| + 1$. Also, in Assumption 3 $a_f = max\{1, \Phi, \alpha_{f_1}, \alpha_{f_2}\}$, which is unknown and estimated, considering (18) and (20). On the other hand, the Nussbaum-type function, used in (19), is selected as,

$$N(\xi) = \xi^2 \cos(\xi), \tag{38}$$

which satisfies Definition 1 conditions. Also, the controller parameters are selected as, $\sigma_0 = 0.1, \sigma_1 = 1$, $\lambda_{D_0} = 1$, $\lambda = 0.1$

1) NORMAL ACTUATION MODE

The performance of the wind turbine in normal actuation situations using the proposed controller (19), the IBC (30), and the MFO-PID (31), under the wind speed profile, shown in Fig. 4, are demonstrated and compared in Figs. 5-8. Faults and uncertainty in the pitch actuator are considered as, $\alpha_{f_1} = \alpha_{f_2} = 0$ and consequently $\Delta\tilde{f}_{PAD} = 0$. Also, $\rho = 1$ and $\Phi = 0$. The numerical performance criteria are summarized in Table 2. The criteria $C1$, $C2$ and $C3$ are significantly decreased compared to IBC and MFO-PID, which demonstrates the advantages of the proposed controller to

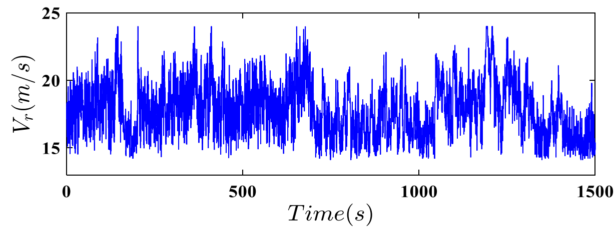

FIGURE 4. Wind speed profile.

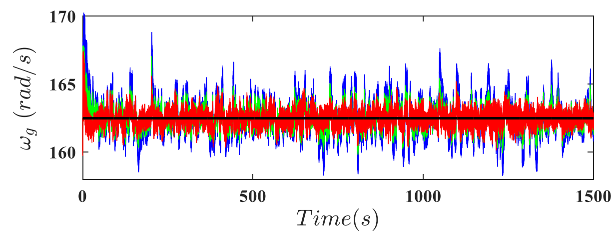

FIGURE 5. Generator speed using IBC (blue line), MFO-PID (green line), proposed controller (red line), and rated generator speed (black line).

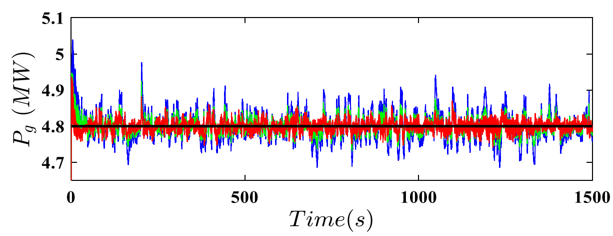

FIGURE 6. Generated power using IBC (blue line), MFO-PID (green line), proposed controller (red line), and rated power (black line).

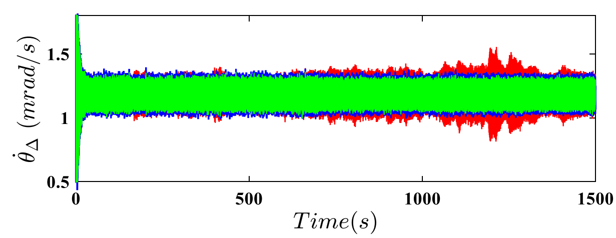

FIGURE 7. Drive train torsion angle rate using IBC (blue line), MFO-PID (green line), proposed controller (red line).

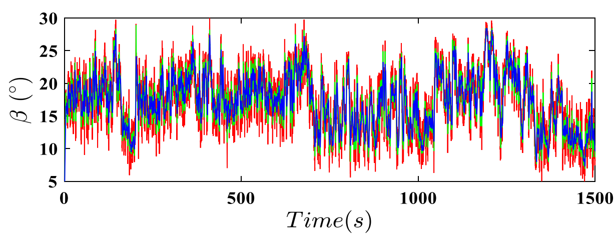

FIGURE 8. Pitch angle using industrial controller (blue line), MFO-PID (green line), and proposed controller (red line).

TABLE 2. Performance criteria in normal situation.

	Proposed controller	MFO-PID	IBC	Unit
$C1$	270.1	851.9	2967	rad^2/s
$C2$	620.1	973.5	2819	GW^2s
$C3$	0.0517	0.0765	0.1437	MW
$C4$	0.002110	0.002102	0.002103	rad^2/s
$C5$	29.05	28.93	28.42	°
$C6$	9.95	9.01	8.53	°/s

produce better rated generator speed and rated power tracking performance. This result is obvious in Figs. 5 and 6. Also, considering Fig. 7, the induced drivetrain torsion angle, i.e. criterion $C4$, using the proposed controller is slightly more than the IBC and MFO-PID controllers. On the other hand, considering Fig. 8 which shows the pitch variation using the proposed controller, i.e. criteria $C5$ and $C6$, are increased, which is expected. Indeed, with high variation of wind speed, having accurately rated power generation, results inevitably in high pitch angle variation.

2) FAULTY ACTUATION MODE

In this section, the operation of the wind turbine system (13), is investigated using both controllers under different pitch actuator faults and dynamic changes, for the wind speed profile given in Fig. 4. It should be noted that, to study the effect of each fault accurately, the pitch actuator faults and dynamic changes are considered separately. Considering (7), pitch actuator bias and effectiveness loss are applied as,

$$\begin{cases} \Phi = 15^\circ, & 200\,(s) \le t \le 600(s) \\ \rho = 0.6, & 900\,(s) \le t \le 1300(s), \end{cases} \tag{39}$$

It should be noted that the $\Delta\tilde{f}_{PAD} = 0$. The generator speed for different time periods, mentioned in (39), using IBC, MFO-PID and proposed controllers are shown in Figs. 9-14. In Fig. 9, the generator speed using IBC in the normal situation and for the pitch bias case, are compared. It is obvious that the pitch bias deviates the generator speed from the rated one, more than the normal case. So, IBC is not able to remove the pitch bias effect and operate the same as the normal situation.

The same result can be obtained considering Fig. 10, in which the effective loss of the pitch actuator is applied.

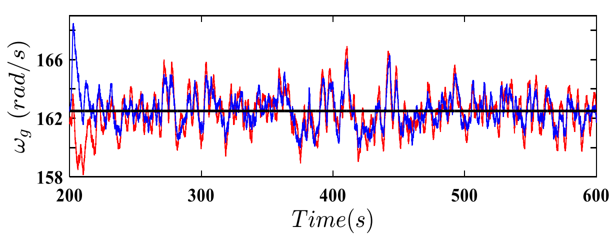

FIGURE 9. Generator speed using IBC in normal actuation case (blue line) and pitch actuator bias case (red line), and rated generator speed (black line).

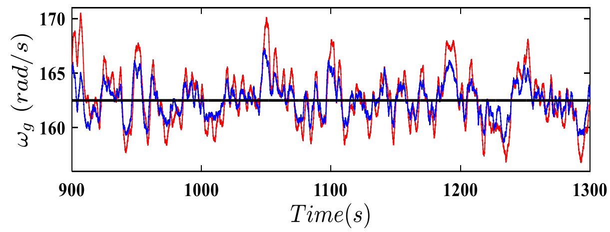

FIGURE 10. Generator speed using IBC in normal actuation case (blue line) and effectiveness loss case (red line), and rated generator speed (green line).

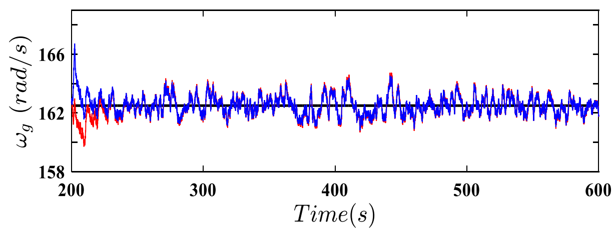

FIGURE 11. Generator speed using MFO-PID in normal actuation case (blue line) and pitch actuator bias case (red line), and rated generator speed (black line).

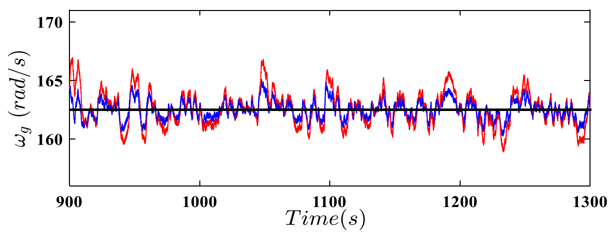

FIGURE 12. Generator speed using MFO-PID in normal actuation case (blue line) and effectiveness loss case (red line), and rated generator speed (black line).

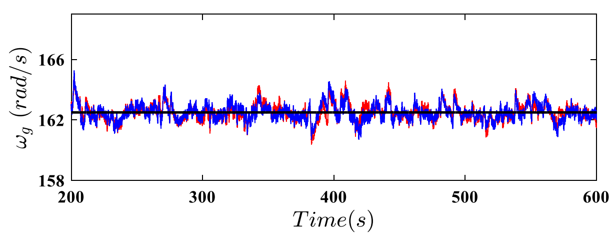

FIGURE 13. Generator speed using proposed controller in normal actuation case (blue line) and pitch actuator bias case (red line), and rated generator speed (black line).

Comparing Figs. 9 and 10, it can be seen that the effectiveness loss is more severe than the pitch bias. In Figs. 11 and 12, the results using MFO-PID are illustrated. The pitch actuator bias has deviated the generator speed from its corresponding value in the normal case, at the beginning of the fault period, compared to the IBC result. However, the effectiveness loss effect is still considerable. Indeed, the optimized gains lead to some degree of tolerance toward the pitch bias, but effectiveness loss effect is severe and not necessarily removed.

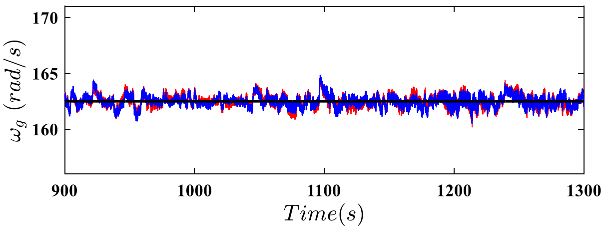

FIGURE 14. Generator speed using proposed controller in normal actuation case (blue line) and effectiveness loss case (red line), and rated generator speed (black line).

In Figs. 13 and 14, the corresponding proposed controller results are illustrated, in which the generator speed with pitch bias and effectiveness loss is obviously kept at the same level as the normal one. Also, comparing Figs. 9, 11 and 13, implies that the proposed controller, in the pitch bias case, is operating more satisfactorily than IBC and MFO-PID. A similar result is also evident comparing Figs. 10, 12 and 14, in the effectiveness loss case. To verify this outcome, the performance criteria are summarized in Table 3.

TABLE 3. Performance criteria in pitch bias and effectiveness loss.

	Proposed controller	MFO-PID	IBC	Unit
$C1$	274.8	1351	4669	rad^2/s
$C2$	643.5	1674	4304	GW^2s
$C3$	0.0776	0.1316	0.2087	MW
$C4$	0.002112	0.002107	0.002105	rad^2/s
$C5$	29.49	28.43	28.34	$^\circ$
$C6$	10	9.24	9.05	$^\circ/s$

Now, the effects of the dynamic change in the pitch actuator are considered. To this end, considering Table 1, the dynamic changes are applied as,

$$\begin{cases} \text{Pump wear}, & 400\,(s) \le t \le 600(s), \\ \text{Hydraulic Leak}, & 700\,(s) \le t \le 900(s), \\ \text{High Air Content}, & 1000\,(s) \le t \le 1200(s), \end{cases} \tag{40}$$

where, in pump wear case $\alpha_{f_1} = 0.63, \alpha_{f_2} = 0.30$, in hydraulic leak case $\alpha_{f_1} = 1, \alpha_{f_2} = 0.88$, and in high air content case $\alpha_{f_1} = 0.81, \alpha_{f_2} = 1$. Also, the pitch actuator dynamic change effect $\Delta\tilde{f}_{PAD}$ is as $\Delta\tilde{f}_{PAD} = -\alpha_{f_1}\Delta(\tilde{\omega}_n^2)\beta - 2\alpha_{f_2}\Delta\left(\tilde{\omega}_n\tilde{\xi}\right)\dot{\beta} + \alpha_{f_1}\Delta(\tilde{\omega}_n^2)\beta_{ref}$, which is an unknown variable, since β, $\dot{\beta}$ and β_{ref} are obtained in the simulation. Considering Fig. 1, it is obvious that all the dynamic changes make the pitch actuator about one second slower. This slower time is not obvious in the time span of the numerical simulation.

So, differences of the pitch angle between the fault free case and the pitch angle in the dynamic change case, are considered as the indicator to accurately study the dynamic change effects, defined as,

$$\Delta\beta = \beta_{dc} - \beta_{normal}, \tag{41}$$

where, β_{dc} represents the pitch angle in the dynamic change case, using the given controller and β_{normal} is the pitch angle in the normal situation using the same controller. Obviously, as long as this indicator is close to zero, it means that the considered controller is able to compensate for the dynamic change effects and keep the pitch angle close to the corresponding one in normal situations. The pitch angle difference using IBC, MFO-PID and the proposed controller, with and without the above-mentioned dynamic changes (40), are demonstrated in Figs. 15-17 for the pump wear case, the hydraulic leak case, and the high air content case, respectively. It is obvious in each dynamic change case that the pitch difference is closer to zero using the proposed controller than for IBC and MFO-PID. This shows the ability of the proposed controller to compensate for the dynamic change in the pitch actuator satisfactorily. Finally, the performance criteria are summarized in Table 4, which confirms the aforementioned results, numerically.

It is very severe if some faults happen simultaneously. Therefore, to evaluate the performance of the proposed controller in this situation, a simultaneous fault scenario is

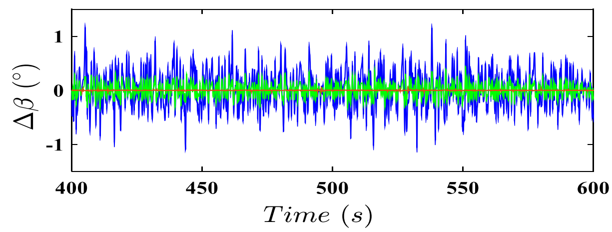

FIGURE 15. Pitch angle difference in normal case and pump wear case using IBC (blue line), MFO-PID (green line), and proposed controller (red line).

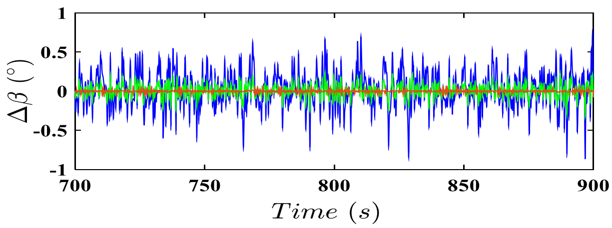

FIGURE 16. Pitch angle difference in normal case and hydraulic leak case using IBC (blue line), MFO-PID (green line), and proposed controller (red line).

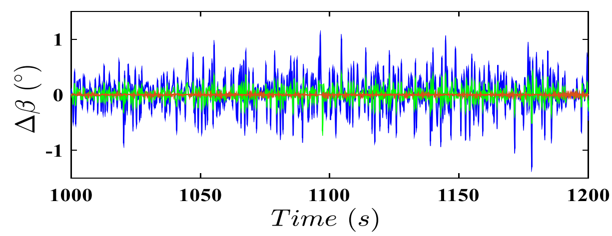

FIGURE 17. Pitch angle difference in normal case and high air content case using IBC (blue line), MFO-PID (green line), and proposed controller (red line).

TABLE 4. Performance criteria in pitch actuator dynamic change case.

	Proposed controller	MFO-PID	IBC	Unit
$C1$	272.1	1031	3257	rad^2/s
$C2$	634.8	1179	2955	GW^2s
$C3$	0.0714	0.1281	0.1720	MW
$C4$	0.002103	0.002099	0.002103	rad^2/s
$C5$	29.18	28.58	28.51	$^\circ$
$C6$	10	10	9.01	$^\circ/s$

applied to the wind turbine as,

$$\begin{cases} \Phi = 10^\circ, & 500\,(s) \le t \le 800(s) \\ \rho = 0.4, & 1000\,(s) \le t \le 1300(s) \end{cases}$$
$$\begin{cases} \text{Pump wear}, & 500\,(s) \le t \le 800(s) \\ \text{Hydraulic Leak}, & 1000\,(s) \le t \le 1300(s), \end{cases} \tag{42}$$

in which, pitch actuator bias and effectiveness loss coincide with pump wear and hydraulic leak cases, respectively. In Figs. 18 and 19, the extracted power using IBC, MFO-PID and the proposed controller in the faulty periods are illustrated. It is obvious that the effectiveness loss and hydraulic leak are very severe, while their effects are satisfactorily accommodated using the proposed controller. Also, the pitch angle difference using IBC, MFO-PID and the proposed controller, with and without the simultaneous fault scenario (42), are demonstrated in Figs. 20 and 21. It is obvious that the proposed controller is tolerant against the considered faults. Finally, the numeric criteria are summarized and compared in Table 5, which shows the appropriate performance of the proposed controller.

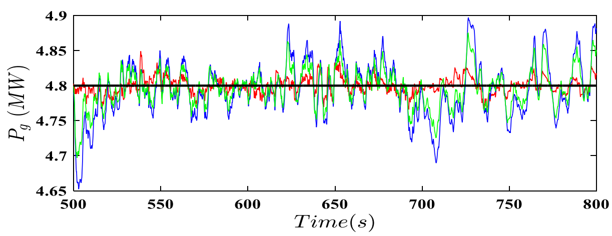

FIGURE 18. Generated power using IBC (blue line), MFO-PID (green line), proposed controller (red line), and rated power (black line), under simultaneous pitch actuator bias and pump wear case.

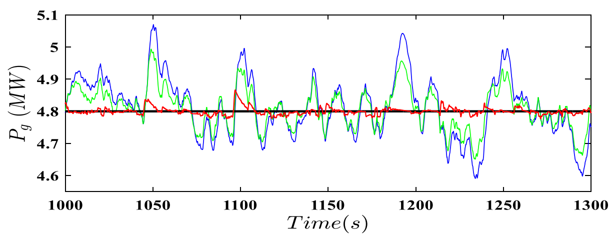

FIGURE 19. Generated power using IBC (blue line), MFO-PID (green line), proposed controller (red line), and rated power (black line), under simultaneous pitch actuator effectiveness loss and hydraulic leak case.

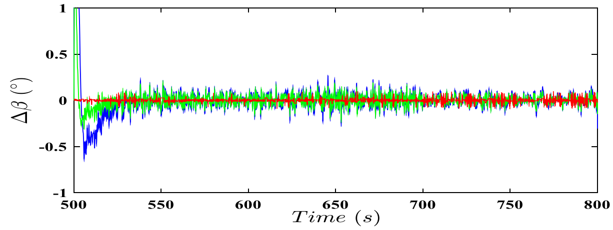

FIGURE 20. Pitch angle difference using IBC (blue line), MFO-PID (green line), and proposed controller (red line), under simultaneous pitch actuator bias and pump wear case.

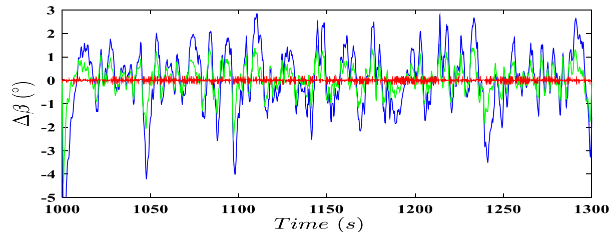

FIGURE 21. Pitch angle difference using IBC (blue line), MFO-PID (green line), and proposed controller (red line), under simultaneous pitch actuator effectiveness loss and hydraulic leak case.

TABLE 5. Performance criteria in pitch actuator dynamic change case.

	Proposed controller	MFO-PID	IBC	Unit
$C1$	268.6	2783	6227	rad^2/s
$C2$	506.8	2701	5706	GW^2s
$C3$	0.0667	0.2003	0.2701	MW
$C4$	0.002203	0.002139	0.002108	rad^2/s
$C5$	29.19	31.94	32.53	$^\circ$
$C6$	10	10	10	$^\circ/s$

VI. DISCUSSION

Our interest in developing new PID control of wind turbines stems from the fact that PID controllers are a key part of almost every practical control system, due to their simplicity in both structure and concept. Accordingly, although the underlying control problem of nonlinear wind turbines is quite difficult, specifically when unknown wind speed and actuation faults are considered, the proposed controller is structurally simple while computationally inexpensive, and functionally effective, as it bears the general PID form.

Differing from conventional PID based methods, the presented control scheme exhibits several distinguishing features. *First*, the designed PID gains consist of two parts, i.e., time-varying part and constant part; the former is consistently and automatically updated without the need for human interference while the latter can be selected freely by the designer. Also, all proportional, integral, and derivative gains are expressly linked to each other through the design parameter λ, thus making the gain tuning process of the presented approach simpler, compared to the traditional PID approach. *Second*, in contrast to most of the PID control systems, which suffer from the lack of guaranteed stability analysis, the proposed algorithm utilized a Lyapunov direct method to provide a systematic procedure to determine PID gains while ensuring the stability of the closed-loop system. By that means, the analytical procedure is delivered to adaptively adjust PID gains without the need for trial and error processes. It is also worth noting that by linking the control gains through λ, the stability analysis is facilitated compared to most of the available PID controls in the literature. *Third*, the presented PID control can handle nonlinearity of the wind turbine models. Also, the presented scheme is adaptive to modeling uncertainties and robust against pitch actuator faults, and wind speed variations. Note that the controller realization is independent of the nonlinear model function. Thus, if the model functions $F(\bullet)$, $G(\bullet)$ and $D(\bullet)$ in (13) change, the designed control strategy will automatically tune the gains to reject the disturbances and compensate for the uncertainties without requiring human interference for adjusting the gains.

VII. CONCLUSION

In this paper, we investigated a novel PID tracking control approach with adaptive gain adjustment for nonlinear wind turbines with unknown pitch actuator characteristics, and unknown wind speed variations. Differing from traditional PID control, the presented scheme adjusts the gains using stability-guaranteed analytic algorithms, thus avoiding manual tuning or frustrating "trial and error" processes. The presented control scheme is capable of automatically accommodating model nonlinearities and uncertainties, undetectable disturbances and pitch actuator faults. Furthermore, the proposed algorithm does not require the process of fault detection, which is very challenging for wind turbines with different sources of noise and uncertainty. Therefore, it can be considered as a practical approach. In addition, in contrast to previous works, it addresses the unknown control direction, as a result of considering an unknown wind speed, by deploying a Nussbaum-type function. The theoretical analysis has verified the proposed controller performance as illustrated from the various numerical simulations. In practice, the proposed method can be used in offshore wind turbines to reduce the need for repetitive and costly maintenance due to pitch actuator faults. Future research directions may include the integration of the controller for both operational regions, with consideration of generator faults.

APPENDIX A

In this appendix, the tower, drivetrain and generator model of wind speed is stated. The applied aerodynamic thrust on the wind turbine tower leads to a bending oscillation and, consequently, the nacelle fore-aft motion. This motion is modelled as [7],

$$M_t\ddot{x}_t = F_t - B_t\dot{x}_t - K_t x_t, \tag{A-1}$$

where, M_t is nacelle mass, B_t is damping ratio and K_t is elasticity coefficient of the tower. Also, x_t is the nacelle displacement, measured from its equilibrium point.

The drivetrain is modelled as a two degree of freedom rotational system. The rotor and generator speeds are input and output speeds of the drivetrain, respectively. Also, inertia of rotor and generator shafts are J_r and J_g, respectively, which are rotating at speeds ω_r and ω_g, respectively. The drivetrain gear meshing, whose ratio is N_g, includes torsion stiffness K_{dt} and torsion damping, B_{dt}.

This elastic gear meshing results in a torsional angle of twist of the main shaft θ_Δ, which is defined as,

$$\theta_\Delta = \theta_r - \theta_g/N_g. \tag{A-2}$$

where, θ_r and θ_g are rotation angles of rotor and generator shafts, respectively. Also, viscous frictions for rotor and generator shaft bearings are considered whose coefficients are B_r and B_g, respectively. The drivetrain efficiency in transferring speed is η_{dt}. Considering all the above mentioned components of the drivetrain, its dynamic behaviour is modelled as [5], [20],

$$\begin{aligned} J_r\dot{\omega}_r &= T_a - K_{dt}\theta_\Delta - (B_r + B_{dt})\,\omega_r + B_{dt}\omega_g/N_g, \\ J_g\dot{\omega}_g &= \eta_{dt}K_{dt}\theta_\Delta/N_g \\ &\quad + \eta_{dt}B_{dt}\omega_r/N_g - (B_g + \eta_{dt}B_{dt}/N_g^2)\omega_g - T_g \\ \dot{\theta}_\Delta &= \omega_r - \omega_g/N_g. \end{aligned} \tag{A-3}$$

The generator and rotor speeds and its derivative are measured by sensors as, $\omega_{g,s} = \omega_g + \nu_{\omega_g}$, $\omega_{r,s} = \omega_r + \nu_{\omega_r}$ and $\dot{\omega}_{r,s} = \dot{\omega}_r + \nu_{\dot{\omega}_r}$, where ν_{ω_g}, ν_{ω_r} and $\nu_{\dot{\omega}_r}$ are noise contents of each sensor [29]. The electrical power is produced in the generator. Also, to adjust the generated power frequency, a converter is located between the generator and grid. Indeed, the current in the generator is controlled utilizing an internal electronic power controller in the converter [7]. Control of demand current in the generator leads to regulation of the torque load on the generator to the reference one, $T_{g,ref}$, commanded by the generator torque controller [20]. The converter is a first order system with time delay τ_g, as,

$$\dot{T}_g = -a_g T_g + a_g T_{g,ref}, \tag{A-4}$$

where, $a_g = 1/\tau_g$. The generator internal electronic controller is much faster than the slow mechanical dynamic behavior of wind turbines. So, the generated electrical power in the generator, P_g, is approximated as a static relation as (3) [7]. Also, the generator torque sensor is modelled as $T_{g,s} = T_g + \nu_{T_{g,s}}$, where $\nu_{T_{g,s}}$ is the sensor noise. Additionally, the limits on generator torque and its variation, are as, $\dot{T}_{g,min} \le \dot{T}_g \le \dot{T}_{g,max}$, $T_{g,min} \le T_g \le T_{g,max}$ [7]. The yaw mechanism of wind turbines is used to change the direction of the blade plane to keep it in the appropriate direction with respect to the wind. In this paper it is assumed that the wind speed direction is perpendicular to the blade plane. So, the dynamic response of the yaw mechanism is ignored. The combined schematic model of the wind turbine is demonstrated in Fig. 22. It should be noted that the generator reference torque is regulated to improve the captured energy, i.e. it is active in the partial load region, and the pitch

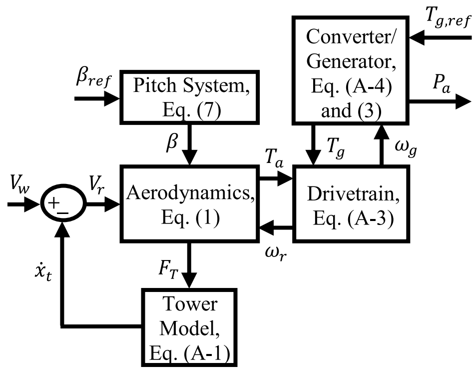

FIGURE 22. Combined schematic model of wind turbine.

angle regulation occurs to maintain the captured power at the nominal value, i.e. it is active in the full load region.

APPENDIX B

In this appendix, the empirical equations for power and thrust coefficients are given. The power coefficient is stated as [20],

$$C_p(\beta, \lambda_{tsr}) = B_1 (B_2/\Lambda - B_3\beta - B_4)\, e^{(-B_5/\Lambda)} + B_6\lambda_{tsr}, \tag{A-5}$$

where, $1/\Lambda = 1/(\lambda_{tsr} + 0.08\beta) - 0.035/(\beta^3 + 1)$, $B_1 = 0.5176$, $B_2 = 116$, $B_3 = 0.4$, $B_4 = 5$, $B_5 = 21$ and $B_6 = 0.0068$ [47]. Also, the thrust coefficient is approximated as [48],

$$\begin{aligned} C_T(\beta, \lambda_{tsr}) &= 0.5\tilde{C}_T\left(1 + sign\left(\tilde{C}_T\right)\right) \\ \tilde{C}_T &= A_1 + A_2(\lambda_{tsr} - A_3\beta)\, e^{-A_4\beta} + A_5\lambda_{tsr}^2 e^{-A_6\beta} \\ &\quad + A_7\lambda_{tsr}^3 e^{-A_8\beta}, \end{aligned} \tag{A-6}$$

where, $A_1 = 0.006$, $A_2 = 0.095$, $A_3 = -4.15$, $A_4 = 2.75$, $A_5 = 0.001$, $A_6 = 7.8$, $A_7 = -0.00016$ and $A_8 = -8.88$. The power and thrust coefficients, using (A-5) and (A-6), are illustrated in Figs. 23 and 24, respectively.

APPENDIX C

In this appendix the numeric values of wind turbine model parameters are given in Table 6 [5].

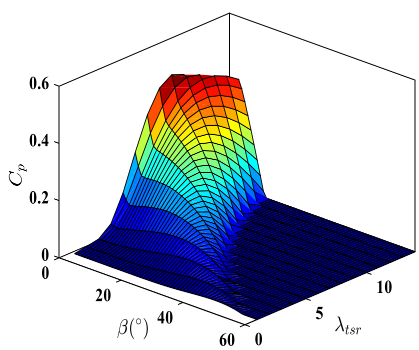

FIGURE 23. Power coefficient surface.

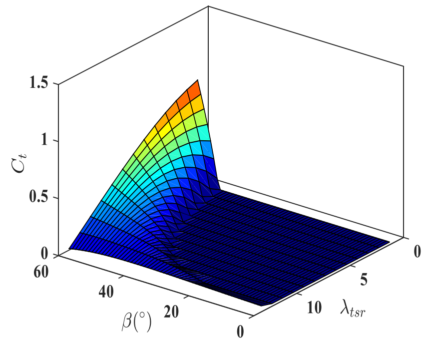

FIGURE 24. Thrust coefficient surface.

TABLE 6. Performance criteria in pitch actuator dynamic change case.

ρ_a	R	J_g	J_r	K_{dt}
1.225 kg/m^3	57.5 m	390 kgm^2	55 $Mkgm^2$	2.7 GNm/rad
B_{dt}	B_g	B_r	N_g	η_{dt}
945 $kNm/(rad/s)$	3.034$Nm/(rad/s)$	27.8 $kNm/(rad/s)$	95	0.97
M_t	B_t	K_t	τ_g	η_g
484 ton	66.7 N/(m/s)	2.55 $MN/$m	0.01 s	0.92
$\dot{T}_{g,min}$	$\dot{T}_{g,max}$	$T_{g,min}$	$T_{g,max}$	ω_n
-50 MNm/s	50 MNm/s	0 Nm	35.3 kNm	11.11 rad/s
ξ	$\dot{\beta}_{min}$	$\dot{\beta}_{max}$	β_{min}	β_{max}
0.6	-10 °/s	10 °/s	-1.9 °	40 °
$P_{g,rated}$	$T_{g,rated}$	$\omega_{g,rated}$	$\omega_{r,rated}$	
4.8 MW	32 kNm	162 rad/s	1.7 rad/s	

REFERENCES

[1] J. Liu, Y. Gao, S. Geng, and L. Wu, "Nonlinear control of variable speed wind turbines via fuzzy techniques," *IEEE Access*, vol. 5, pp. 27–34, 2017.
[2] J. G. Njiri and D. Söffker, "State-of-the-art in wind turbine control: Trends and challenges," *Renew. Sustain. Energy Rev.*, vol. 60, pp. 377–393, Jul. 2016.
[3] H. Habibi, A. Y. Koma, and I. Howard, "Power improvement of non-linear wind turbines during partial load operation using fuzzy inference control," *Control Eng. Appl. Inf.*, vol. 19, no. 2, pp. 31–42, 2017.
[4] J. Lan, R. J. Patton, and X. Zhu, "Fault-tolerant wind turbine pitch control using adaptive sliding mode estimation," *Renew. Energ.*, vol. 119, pp. 219–231, Feb. 2018.
[5] P. F. Odgaard and J. Stoustrup, "A benchmark evaluation of fault tolerant wind turbine control concepts," *IEEE Trans. Control Syst. Technol.*, vol. 23, no. 3, pp. 1221–1228, May 2015.
[6] Y. Song, X. Huang, and C. Wen, "Robust adaptive fault-tolerant PID control of MIMO nonlinear systems with unknown control direction," *IEEE Trans. Ind. Electron.*, vol. 64, no. 6, pp. 4876–4884, Jun. 2017.
[7] C. Sloth, T. Esbensen, and J. Stoustrup, "Robust and fault-tolerant linear parameter-varying control of wind turbines," *Mechatronics*, vol. 21, no. 4, pp. 645–659, Jun. 2011.
[8] H. Habibi, I. Howard, and R. Habibi, "Bayesian sensor fault detection in a Markov jump system," *Asian J. Control*, vol. 19, no. 4, pp. 1465–1481, 2017.
[9] H. Jafarnejadsani, J. Pieper, and J. Ehlers, "Adaptive control of a variable-speed variable-pitch wind turbine using radial-basis function neural network," *IEEE Trans. Control Syst. Technol.*, vol. 21, no. 6, pp. 2264–2272, Nov. 2013.
[10] H. Habibi, H. R. Nohooji, and I. Howard, "Constrained control of wind turbines for power regulation in full load operation," in *Proc. 11th Asian Control Conf. (ASCC)*, Dec. 2017, pp. 2813–2818.

[11] U. Giger, P. Kühne, and H. Schulte, "Fault tolerant and optimal control of wind turbines with distributed high-speed generators," *Energies*, vol. 10, no. 2, pp. 1–13, 2017.
[12] H. Jafarnejadsani, "L1-optimal control of variable-speed variable-pitch wind turbines," M.S. thesis, Dept. Mech. Eng., Univ. Calgary, Calgary, AB, Canada, 2013.
[13] L.-L. Fan and Y.-D. Song, "Neuro-adaptive model-reference fault-tolerant control with application to wind turbines," *IET Control Theory Appl.*, vol. 6, no. 4, pp. 475–486, Mar. 2012.
[14] F. Jaramillo-Lopez, G. Kenne, and F. Lamnabhi-Lagarrigue, "A novel online training neural network-based algorithm for wind speed estimation and adaptive control of PMSG wind turbine system for maximum power extraction," *Renew. Energy*, vol. 86, pp. 38–48, Feb. 2016.
[15] Y.-M. Kim, "Robust data driven H-infinity control for wind turbine," *J. Franklin Inst.*, vol. 353, no. 13, pp. 3104–3117, Sep. 2016.
[16] H. Badihi, Y. Zhang, and H. Hong, "Wind turbine fault diagnosis and fault-tolerant torque load control against actuator faults," *IEEE Trans. Control Syst. Technol.*, vol. 23, no. 4, pp. 1351–1372, Jul. 2015.
[17] H. Habibi, A. Y. Koma, and A. Sharifian, "Power and velocity control of wind turbines by adaptive fuzzy controller during full load operation," *Iran. J. Fuzzy Syst.*, vol. 13, no. 3, pp. 35–48, 2016.
[18] R. Tiwari and N. Babu, "Recent developments of control strategies for wind energy conversion system," *Renew. Sustain. Energy. Rev.*, vol. 66, pp. 268–285, Dec. 2016.
[19] A. G. Aissaoui, A. Tahour, N. Essounbouli, F. Nollet, M. Abid, and M. I. Chergui, "A Fuzzy-PI control to extract an optimal power from wind turbine," *Energy Convers. Manage.*, vol. 65, pp. 688–696, Jan. 2013.
[20] H. Habibi, H. R. Nohooji, and I. Howard, "Power maximization of variable-speed variable-pitch wind turbines using passive adaptive neural fault tolerant control," *Frontiers Mech. Eng.*, vol. 12, no. 3, pp. 377–388, Sep. 2017.
[21] S. Simani, S. Farsoni, and P. Castaldi, "Fault diagnosis of a wind turbine benchmark via identified fuzzy models," *IEEE Trans. Ind. Electron.*, vol. 62, no. 6, pp. 3775–3782, Jun. 2015.
[22] H. Badihi, Y. Zhang, and H. Hong, "Fuzzy gain-scheduled active fault-tolerant control of a wind turbine," *J. Franklin Inst.*, vol. 351, no. 7, pp. 3677–3706, Jul. 2014.
[23] S. Cho, Z. Gao, and T. Moan, "Model-based fault detection, fault isolation and fault-tolerant control of a blade pitch system in floating wind turbines," *Renew. Energy*, vol. 120, pp. 306–321, May 2018.
[24] P. Kühne, F. Pöschke, and H. Schulte, "Fault estimation and fault-tolerant control of the FAST NREL 5-MW reference wind turbine using a proportional multi-integral observer," *Int. J. Adapt. Control Signal Process.*, vol. 32, no. 4, pp. 568–585, 2018.
[25] S. Abdelmalek, A. T. Azar, and D. Dib, "A novel actuator fault-tolerant control strategy of DFIG-based wind turbines using Takagi-Sugeno multiple models," *Int. J. Control Autom.*, vol. 16, no. 3, pp. 1415–1424, Jun. 2018.
[26] H. Badihi, Y. Zhang, and H. Hong, "Fault-tolerant cooperative control in an offshore wind farm using model-free and model-based fault detection and diagnosis approaches," *Appl. Energ.*, vol. 201, pp. 284–307, Sep. 2017.
[27] H. Sanchez, T. Escobet, V. Puig, and P. F. Odgaard, "Fault diagnosis of an advanced wind turbine benchmark using interval-based ARRs and observers," *IEEE Trans. Ind. Electron.*, vol. 62, no. 6, pp. 3783–3793, Jun. 2015.
[28] P. F. Odgaard, J. Stoustrup, and M. Kinnaert, "Fault-tolerant control of wind turbines: A benchmark model," *IEEE Trans. Control Syst. Technol.*, vol. 21, no. 4, pp. 1168–1182, Jul. 2013.
[29] S. M. Tabatabaeipour, P. F. Odgaard, T. Bak, and J. Stoustrup, "Fault detection of wind turbines with uncertain parameters: A set-membership approach," *Energies*, vol. 5, no. 7, pp. 2424–2448, 2012.
[30] H. Habibi, H. R. Nohooji, and I. Howard, "Optimum efficiency control of a wind turbine with unknown desired trajectory and actuator faults," *J. Renew. Sustain. Energy*, vol. 9, no. 6, p. 063305, 2017.
[31] H. Habibi, H. R. Nohooji, and I. Howard, "A neuro-adaptive maximum power tracking control of variable speed wind turbines with actuator faults," in *Proc. Austral. New Zealand Control Conf. (ANZCC)*, Dec. 2017, pp. 63–68.
[32] C. Sloth, T. Esbensen, and J. Stoustrup, "Active and passive fault-tolerant LPV control of wind turbines," in *Proc. Amer. Control Conf. (ACC)*, Jun./Jul. 2010, pp. 4640–4646.
[33] F. D. Bianchi, R. Sánchez-Peña, and M. Guadayol, "Gain scheduled control based on high fidelity local wind turbine models," *Renew. Energy*, vol. 37, no. 1, pp. 233–240, Jan. 2012.
[34] K. Z. Østergaard, J. Stoustrup, and P. Brath, "Linear parameter varying control of wind turbines covering both partial load and full load conditions," *Int. J. Robust Nonlinear Control*, vol. 19, no. 1, pp. 92–116, 2009.
[35] Y. Qi and Q. Meng, "The application of fuzzy PID control in pitch wind turbine," *Energy Procedia*, vol. 16, pp. 1635–1641, Jan. 2012. [Online]. Available: http://www.sciencedirect.com/science/article/pii/S1876610212002640, doi: 10.1016/j.egypro.2012.01.254.
[36] B. Boukhezzar and H. Siguerdidjane, "Nonlinear control of a variable-speed wind turbine using a two-mass model," *IEEE Trans. Energy Convers.*, vol. 26, no. 1, pp. 149–162, Mar. 2011.
[37] T. D. Do, "Disturbance observer-based fuzzy SMC of WECSs without wind speed measurement," *IEEE Access*, vol. 5, pp. 147–155, Nov. 2016.
[38] D. Song, J. Yang, Z. Cai, M. Dong, M. Su, and Y. Wang, "Wind estimation with a non-standard extended Kalman filter and its application on maximum power extraction for variable speed wind turbines," *Appl. Energ.*, vol. 190, pp. 670–685, Mar. 2017.
[39] Y. Song, Z. Zhang, P. Li, W. Wang, and M. Qin, "Robust adaptive variable speed control of wind power systems without wind speed measurement," *J. Renew. Sustain. Energy*, vol. 5, no. 6, p. 063115, 2013.
[40] S. Simani, "Overview of modelling and advanced control strategies for wind turbine systems," *Energies*, vol. 8, no. 12, pp. 13395–13418, 2015.
[41] V. Petrović, M. Jelavić, and M. Baotić, "Advanced control algorithms for reduction of wind turbine structural loads," *Renew. Energy*, vol. 76, pp. 418–431, Apr. 2015.
[42] Y. Song, X. Huang, and C. Wen, "Tracking control for a class of unknown nonsquare MIMO nonaffine systems: A deep-rooted information based robust adaptive approach," *IEEE Trans. Autom. Control*, vol. 61, no. 10, pp. 3227–3233, Oct. 2016.
[43] H. K. Khalil, "Universal integral controllers for minimum-phase nonlinear systems," *IEEE Trans. Autom. Control*, vol. 45, no. 3, pp. 490–494, Mar. 2000.
[44] S. S. Ge, F. Hong, and T. H. Lee, "Adaptive neural control of nonlinear time-delay systems with unknown virtual control coefficients," *IEEE Trans. Syst., Man, Cybern. B, Cybern.*, vol. 34, no. 1, pp. 499–516, Feb. 2004.
[45] M. A. Ebrahim, M. Becherif, and A. Y. Abdelaziz, "Dynamic performance enhancement for wind energy conversion system using moth-flame optimization based blade pitch controller," *Sustain. Energy Technol. Assessments*, vol. 27, pp. 206–212, Jun. 2018.
[46] D. Wu, W. Liu, J. Song, and Y. She, "Fault estimation and fault-tolerant control of wind turbines using the SDW-LSI algorithm," *IEEE Access*, vol. 4, pp. 7223–7231, Oct. 2016.
[47] H. Ren *et al.*, "A novel constant output powers compound control strategy for variable-speed variable-pitch wind turbines," *IEEE Access*, vol. 6, pp. 17050–17059, 2018, doi: 10.1109/ACCESS.2018.2801458.
[48] S. Georg, H. Schulte, and H. Aschemann, "Control-oriented modelling of wind turbines using a Takagi–Sugeno model structure," in *Proc. IEEE Int. Conf. Fuzzy Syst. (FUZZ-IEEE)*, Jun. 2012, pp. 1–8.

HAMED HABIBI received the B.Sc. degree from Khaje Nasir University, Tehran, Iran, in 2010, and the M.Sc. degree from the University of Tehran, Tehran, in 2013, all in mechanical engineering. He is currently pursuing the Ph.D. degree with Curtin University, Perth, Australia. His current research interests include control systems, fault detection, isolation, identification, accommodation, and fault tolerant control with applications on wind turbines.

HAMED RAHIMI NOHOOJI received the Ph.D. degree in mechanical engineering from Curtin University, Australia, in 2018. Before joining Curtin University, he was a Lecturer at Islamic Azad University, Damavand, Iran, and also a Researcher at the University of Pisa, Italy. He was a Visiting Research Scholar with the University of Birmingham, U.K., in 2017. He is currently a Post-Doctoral Research Fellow with the Université catholique de Louvain, Belgium. His current research interests include the field of dynamic systems and control, human–robot interaction, and robotic rehabilitation.

IAN HOWARD received the bachelor's and Ph.D. degrees in mechanical engineering from The University of Western Australia in 1984 and 1988, respectively. He was with the Defense Science and Technology Organization for five years. In 1994, he joined Curtin University as a Lecturer in applied mechanics and dynamic systems, where he was promoted to Full Professor in 2016 and continues to supervise research in the dynamic behavior of rotating machinery for fault detection and classification for industry applications.